High Energy Antiproton–Proton Collisions The Collider Detector at Fermilab

George W. Brandenburg

Harvard University High Energy Physics Laboratory
42 Oxford Street, Cambridge, Mass. 02138, USA

Abstract. Recent results from experiments at antiproton-proton colliders are presented with emphasis on those from the Collider Detector at Fermilab (CDF). The data on hadron jet, W, and Z production are all in excellent agreement with the standard model. The lower limit for the top quark mass is found to be somewhat above the W mass. No evidence is found for W' or Z' states or for supersymmetric particles.

1. Introduction

Antiproton–proton collider experiments have provided very exciting data during the 1980's. From the initial discovery of the W and Z bosons at CERN through the continuing search for the top quark at Fermilab, there has been a wealth of information from these experiments – thus far all in excellent agreement with the Standard Model. In the decade to come these experiments together with those at LEP will continue to apply stringent tests within the Standard Model and to look for exciting new effects beyond it.

In this talk I will take a brief look at the accelerators and experiments that have made this work possible and then summarize the most recent results. I will concentrate primarily on results from my own experiment, CDF, reviewing the following major topics: Jet/QCD studies (section 4), W/Z physics (section 5), and finally the top quark search (section 6). In each of the physics sections I will try to project what can be expected from future data – of course that which is unexpected may prove to be the most exciting!

2. Hadron Colliders – the Tevatron

The key element which has made the study of high energy antiproton–proton collisions possible was the development of the hadron collider. The first such machine was the CERN ISR, but the development of the SPS collider together with its antiproton source by Van de Meer, Rubbia, and others opened the current epoch of experimentation. This machine was followed by the Fermilab Tevatron collider, which used similar techniques for the production and cooling of antiprotons. However, Fermilab was able to utilize the superconducting Tevatron as a storage ring allowing higher energies than the SPS ring with its conventional magnets. I will describe the main features of the Fermilab system below.

Pub. Proceedings Yukawa Memorial Symposium, Nishinomiya, Japan

The first step is the production of antiprotons. This is done using 120 GeV protons from the old Fermilab main ring, incident on a lithium target. Antiprotons are filtered from the resulting debris and are channeled into an 8 GeV pair of rings called the Debuncher/Accumulator. Here the antiprotons are stochastically "cooled" such that the phase space they occupy will easily fit within the available phase space of the larger rings. It takes several hours to accumulate in excess of 10^{11} antiprotons, at which point they can be transferred in six bunches to the Tevatron ring.

Once the six bunches of antiprotons have been inserted into the Tevatron it is a relatively straightforward matter to also insert six comparable bunches of protons directly from the old main ring. With the antiprotons and protons inserted and rotating in opposite directions, the Tevatron is gently raised from its injection energy of 150 GeV to its maximum energy of 900 GeV. The two sets of six bunches pass each other at twelve points around the circumference of the ring, however, the beams are only focussed to a collision point where an experiment has been installed. Previously CDF has been the only major experiment taking data (at the "B0" collision point), while in the upcoming run CDF will be joined by the new D0 experiment.

In the previous Tevatron collider run lasting from July 1988 to July 1989 the machine delivered a total integrated luminosity of 9 pb^{-1} at a collision energy of $\sqrt{s}$ = 1800 GeV, and the CDF experiment was able to log approximately half of this to tape. (Delivered luminosity is stated in units of inverse cross section – when multiplied times the cross section for a process one obtains the expected number of associated events.) Fermilab plans to run the Tevatron collider at approximately two year intervals through the 1990's making improvements each time. Some of the projected improvements are: install electrostatic separators to reduce beam–beam interactions at unused crossing points, increase the number of bunches (20–40), raise the Tevatron energy to 1000 GeV, and replace the old main ring with a more efficient Main Injector in a separate tunnel. With these improvements the delivered luminosity can be expected to increase by a factor of roughly five in each successive run. Thus we can expect between 25 and 50 pb^{-1} in the CDF/D0 run starting next summer.

It is important to note that increased luminosity at a hadron collider is practically speaking almost as valuable as increased energy. The most interesting processes require very high energy parton–parton interactions. Because of the rapid decrease of the proton structure function with increasing parton momentum fraction, larger luminosity results in a measureable rate for ever higher energy parton–parton collisions.

3. The Experiments – CDF

The experiments which have been designed to study high energy hadron collisions have to take advantage of two important aspects of the most interesting interactions. First these processes tend to involve large masses and momentum transfers, so the experiments should emphasize measurement of outgoing particles at large angles. Second the interesting

massive objects tend to decay weakly, so it is important to be able to identify leptons. Thus the most important components are tracking to identify the trajectories of muons and electrons, segmented calorimetry to measure the energy of electrons and quark jets, and complete calorimetric coverage to infer the presence of neutrinos.

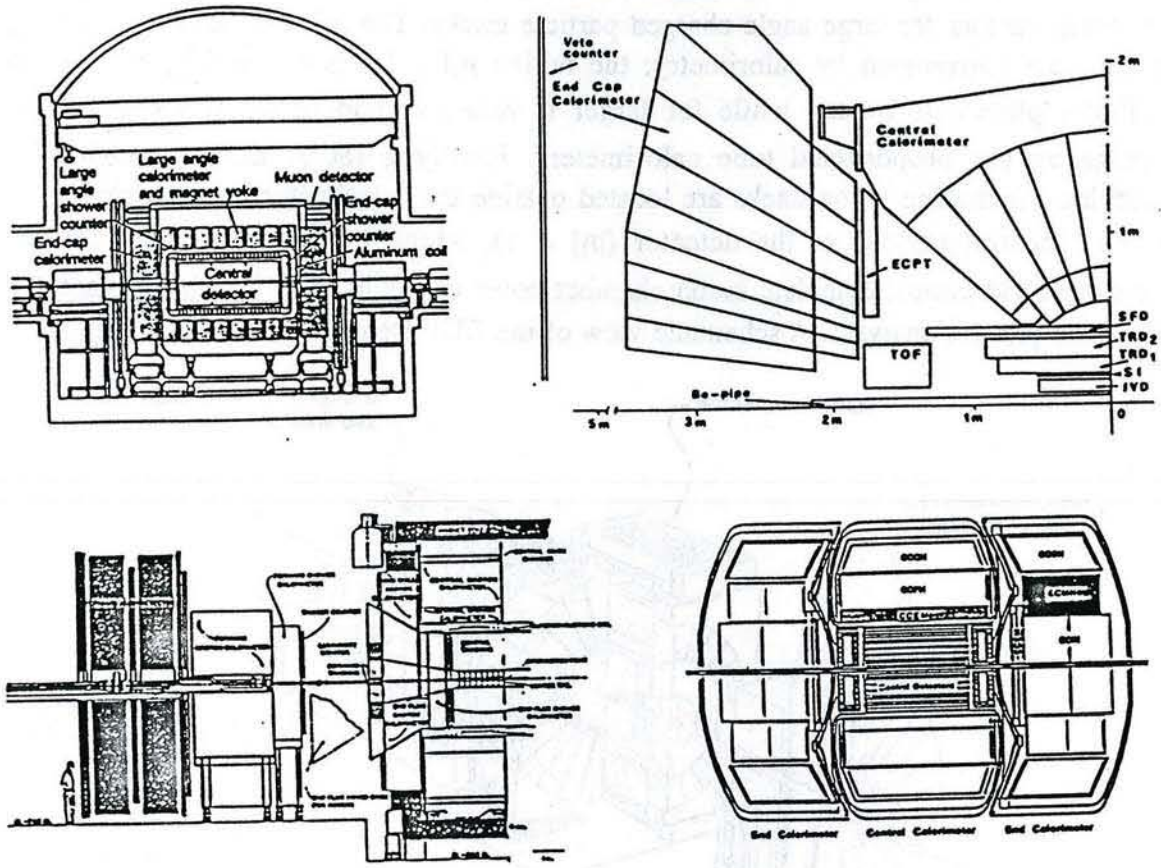

Figure 1 The four major $\bar{p}$–p collider experiments: UA1 (upper left) and UA2 (upper right) at CERN, CDF (lower left) and D0 (lower right) at Fermilab.

Fig. 1. shows the major detectors that have been or will be used to study antiproton–proton collisions. The original two CERN detectors complemented each other in that both had the major features pointed out above, but UA1 emphasized particle tracking in a dipole field while UA2 emphasized segmented calorimetry for electron and jet measurement. The Collider Detector at Fermilab (CDF) has both excellent particle tracking in a solenoidal field and very good calorimetry. However, the new Fermilab detector, D0, will be highlighted by a liquid argon calorimeter which will provide even better energy measurement. The UA1, UA2 program at CERN is now winding down, but CDF and D0 will begin major new data taking runs at Fermilab in the summer of 1991.

Because I will be focussing primarily on results from the CDF detector I will describe its components in somewhat more detail [1]. The sections of the detector are logically divided into different pseudorapidity regions, where this familiar approximation for the longitudinal rapidity variable is given by $\eta = \ln(\tan(\theta/2))$. The innermost element is a

vertex time–projection chamber which is used to accurately locate the event vertex along the beam line and to ensure that there are not multiple interactions. Surrounding the vertex chamber is an 84 layer cylindrical drift chamber which extends out to a radius of 1.3 m and covers the interval $-1.0 < \eta < +1.0$. The tracking chambers are enclosed in a superconducting magnet with an axial field of 1.5 Tesla, resulting in the accurate measurement of the momentum vectors for large angle charged particle tracks. The solenoid and the tracking chambers are surrounded by calorimetry: the region $|\eta| < 1.1$ is covered by segmented scintillator plate calorimeter, while for larger η values extending to $|\eta| = 4.2$ there is coverage by gas proportional tube calorimeters. Finally a set of drift chambers for identifying penetrating muon tracks are located outside the calorimeter in the region $|\eta| < 0.6$. The "central region" of the detector ($|\eta| < 1$), which includes particle tracking, calorimetry, and almost complete muon chamber coverage, is used as a starting place for most of the physics analyses. A schematic view of the CDF Detector is shown in Fig. 2.

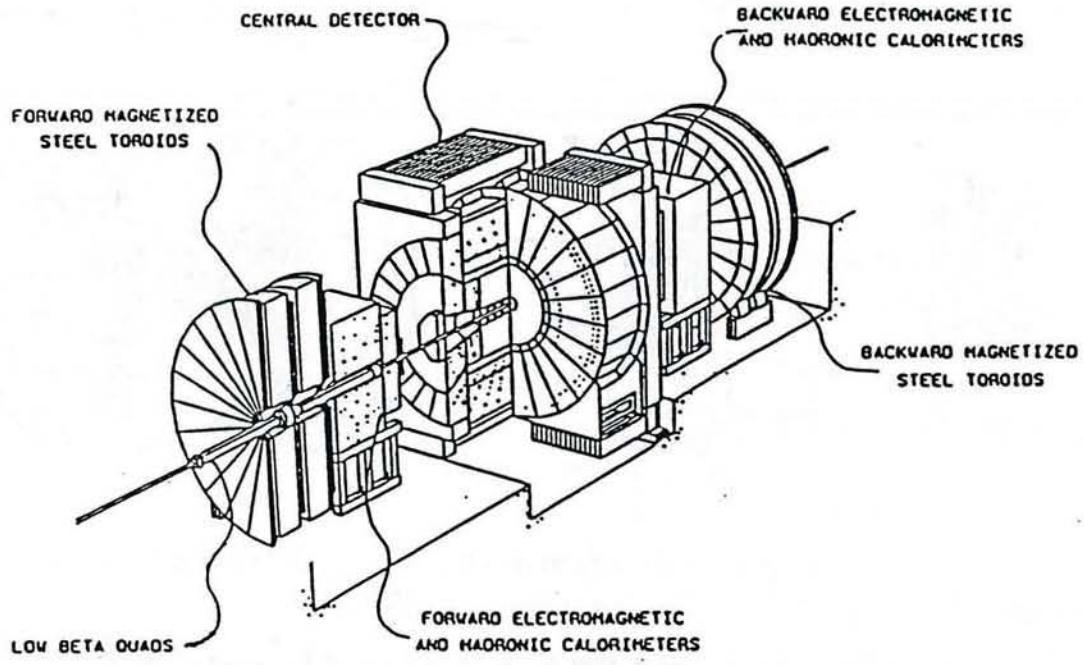

Figure 2 A schematic drawing of the CDF detector.

Because the rates for uninteresting processes tend to be astronomically large, it is necessary to have an elaborate, very fast trigger scheme to sort out the most interesting events for further analysis. Typical event signatures that can be used in this trigger are clusters of calorimeter energy representing electrons or parton jets, penetrating tracks from muons, and a large value of the "missing transverse energy". (Transverse energy is defined in analogy to transverse momentum as $E_T = E \sin(\theta)$, where E is the energy of a calorimeter cluster. Assuming that the vector sum of the outgoing E_T for all particles is approximately zero, the missing E_T is defined as the negative of the total observed E_T summed over all calorimeter segments.)

In CDF the trigger is subdivided into four logical levels. An event must pass the lower levels to reach the higher levels. The lower levels are simple topologically and hence very fast, while the higher levels are more complicated and introduce "dead time" into the experiment. The highest level consists of a complete event reconstruction on a "farm" of on–line microprocessors. Table 1 summarizes the CDF trigger system and the size of the interaction cross section that was accepted by each level in the last run. The net result of this trigger scheme was to reduce a primary event rate of 80 khz down to a final data stream of approximately 2 events per second. It should be noted that the final data set always includes random samplings of the more prolific processes as well as all of the most exotic triggers.

Table 1

CDF Trigger Levels

Level	Cross Section	Description
0	45 mb	Beam–beam interactions
1	1 mb	Simple calorimeter energy sums
2	3 μb	Topological combinations (30 flavors)
3	1 μb	Event reconstruction and tracking

Just as the the accelerators are upgraded between major runs, the detectors must keep pace with their own improvements. Some of these are dictated by the demands placed on the system by the projected increases in luminosity. Other improvements are designed to enhance the ability of the detectors to study various processes. For the next Tevatron run a number of upgrades are being carried out at CDF. There are several readout electronics improvements designed to accommodate higher luminosity. The level 3 trigger system is being rebuilt with more powerful microprocessors (MIPS R3000's). A silicon vertex detector is being added around the beam pipe to allow the tagging of B decays. A preradiator layer is being added in front of the central calorimeters to aid in the identification of direct photons. Finally the central muon system is being enhanced with additional steel to eliminate hadron "punch–through" and with additional chambers to extend its angular coverage. The latter improvements will be very useful for particle searches as well as for electroweak studies. In future runs CDF will further extend its muon coverage and will replace its gas tube calorimeters with faster scintillator tile versions.

4. Jets Physics – QCD

It is assumed that free quarks and gluons never emerge from a hadronic interaction, and that instead one sees collimated "jets" of particles which result from the hadronization of the partons. Such jets were originally observed in electron–positron collider experiments as a statistical elongation of the overall angular distribution of the outgoing particles. Now in high energy hadron collider experiments jets appear as highly collimated clusters of

particles which stand out distinctly from one another. They can be most dramatically observed in a two dimensional histogram ("lego plot") of the transverse energy deposited in the calorimeters, where the two axes are the pseudorapidity, η, and the azimuth angle, ϕ. In Fig. 3 a lego plot for a high energy elastic parton–parton scatter is shown. The jets representing the two outgoing partons must be back-to-back in azimuth, but may occur at any pseudorapidity values as the incoming partons have their longitudinal momenta statistically distributed according to the structure functions.

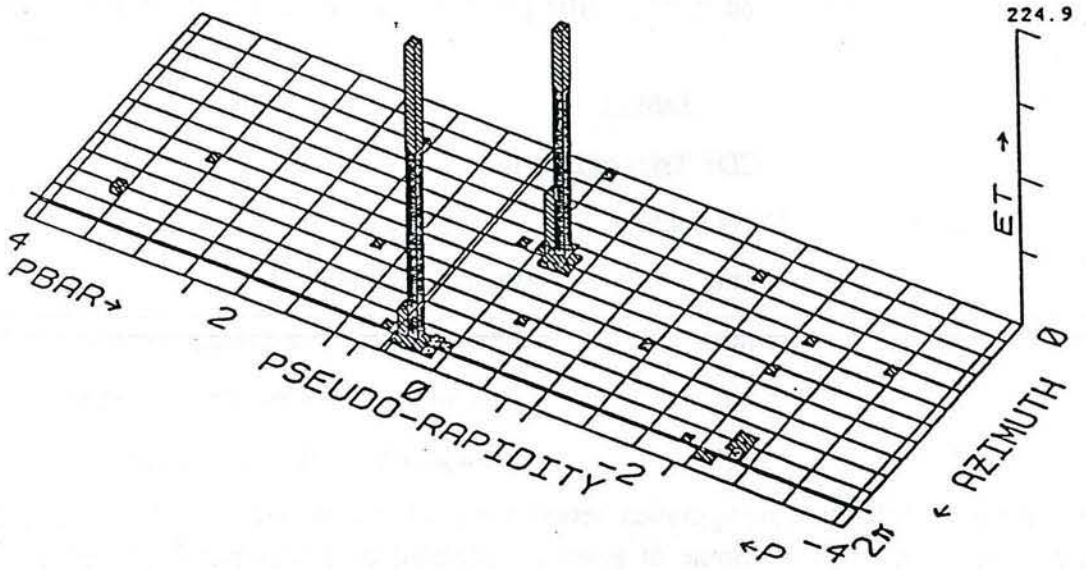

Figure 3 A lego plot of two jet event from CDF.

As can be seen from the figure it is a relatively easy matter to select the jets by defining a small area on the surface of the lego plot containing most of the jet energy. It is important to note that the product $dE_T^2\, d\eta\, d\phi$ is the element of invariant phase space, and as a consequence jets will have a symmetric E_T profile in the η–ϕ plane. In fact selecting the energy inside a circular contour centered on a jet is similar to selecting only those jet fragments with with η_{jet} above a certain limit, where η_{jet} is calculated with respect to the jet axis instead of the beam axis. For example our CDF jet selection algorithm uses a circular area of radius, $R_{\eta\phi} = 0.7$, which corresponds to an approximate η_{jet} lower limit of 1.0. Thus at most a few low energy fragments of a jet will be missed by the algorithm. Nonetheless is is necessary to correct the resulting jet energy for such losses as well as for losses due to geometric gaps in the calorimeter and for the overall calibration of the calorimeter energy scale.

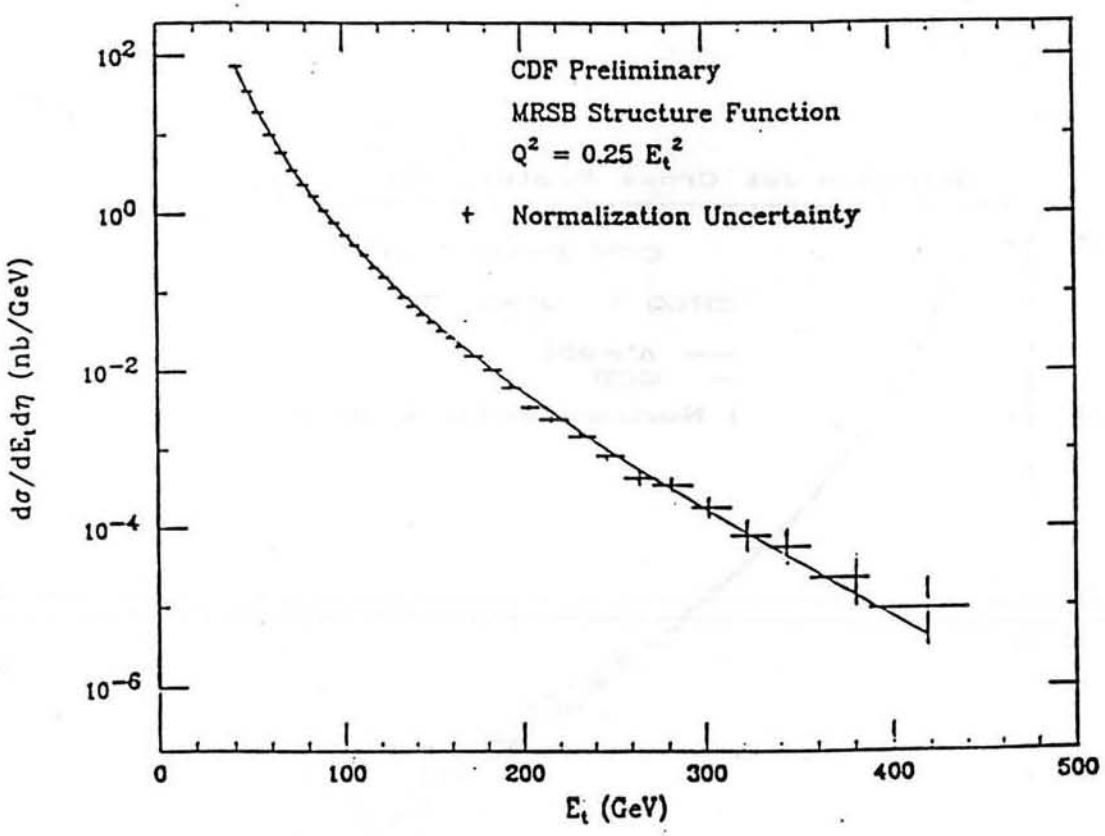

Figure 4 The inclusive jet differential cross section as a function of E_T from CDF ($\sqrt{s}$ = 1800 GeV). The curve is the NLO QCD prediction of Ellis, Kunst and Soper.

The most recent CDF inclusive cross section is shown as a function of E_T in Fig. 4 for jets in the central region as selected by the above algorithm. The data falls almost seven orders of magnitude from $E_T \approx 20$ GeV to $E_T \approx 400$ GeV. It is shown in comparison with the Next to Leading Order QCD calculation of Ellis, Kunst and Soper [2], where the QCD prediction has been absolutely normalized to the data. The agreement between theory and experiment is remarkable.

The same data are shown in Fig. 5, but this time compared instead to a lowest order QCD calculation plus a contact term representing possible quark compositeness. The contact term is proportional to $1/\Lambda^2$, where is Λ is the compositeness energy scale. At the 95% confidence level only values of Λ greater than 950 GeV are consistent with the data. The corresponding distance scale is less than $2 \cdot 10^{-17}$ cm or 0.0002 fermi. It is interested to note that the length and distance scales addressed by Yukawa some fifty years ago differed from these by a factor of roughly 5000. In the next CDF run it should be possible to extend the measurement of the inclusive jet spectrum beyond $E_T = 500$ GeV and to extend the compositeness scale limit beyond 1200 GeV.

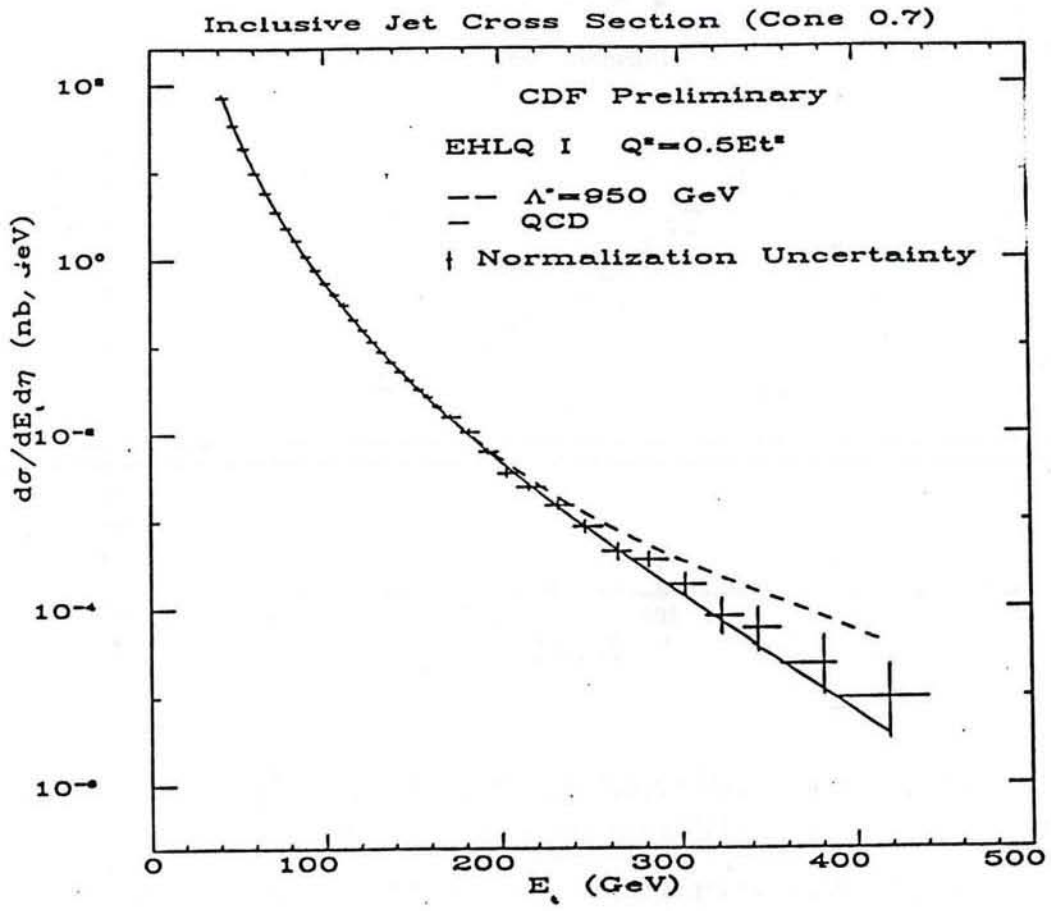

Figure 5 The inclusive jet differential cross section as a function of E_T from CDF ($\sqrt{s}$ = 1800 GeV). The curves are lowest order QCD plus quark compositeness terms.

The primary component of the inclusive jet cross section are the dijet events which represent parton–parton elastic scattering. The angular distribution for these events has also been measured and is displayed in Fig. 6 as a function of $\chi = (1+\cos\theta^*)/(1-\cos\theta^*)$, where θ^* is Collins–Soper approximation of the center–of–mass scattering angle [3]. The χ distribution would be approximately flat for $\chi > 2$ in the case of simple Rutherford scattering, but is modified by higher order corrections. The figure is divided into a two parts by the dijet mass; the high dijet mass part is the one where one would expect to see deviations from QCD. The curves shown are for QCD plus a contact term as in Fig. 5, and the results obtained here are consistent with those from the inclusive spectrum.

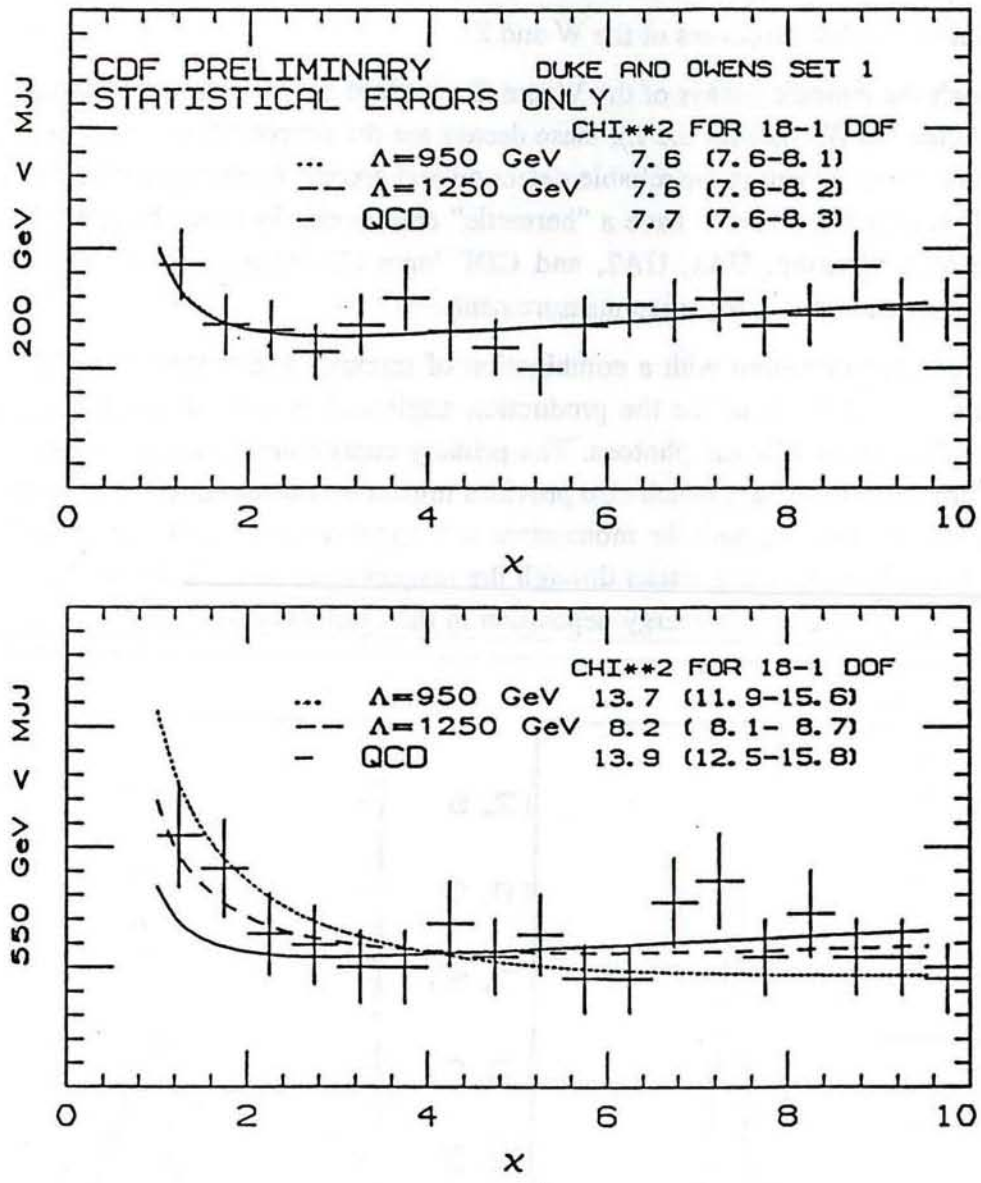

Figure 6 The dijet angular distribution from CDF as a function of $\chi = (1+\cos\theta^*)/(1-\cos\theta^*)$.

There are studies also underway of the CDF data for multijet events. Events with as many as six jets have been observed, and thus far these data have proven to be completely consistent with the predictions of QCD.

5. Electroweak Physics - W,Z Production

The intermediate gauge bosons, although long predicted, were first directly observed by UA1 and UA2 at CERN [4]. Although the Z has also been seen and has had its properties precisely measured at LEP, study of the W remains the domain of hadron colliders. In this section I will review the results on the Z and present the most recent measurement of the W

mass. I will also discuss the determination of the mixing parameter, $\sin^2\theta_W$, and the measurement of other properties of the W and Z.

Although the leptonic decays of the W and Z represent only a small fraction of their total width (1/6 for the W, 1/20 for the Z), these decays are the simplest topologies to detect. The key to their measurement is the reliable detection and precise measurement of electrons and muons. It is also important to have a "hermetic" calorimeter in order to infer the possible presence of a neutrino. UA1, UA2, and CDF have all devoted considerable effort to understanding and calibrating these measurements.

Electrons are measured with a combination of tracking and calorimetry. The tracking provides a measurement of the the production angle and is used to discriminate against backgrounds such as π^0's and photons. The primary energy measurement for the electrons comes from the calorimetry, which also provides rejection of charged hadrons. In the case of muons tracking provides both the momentum and angle measurement. Muon backgrounds are eliminated by connecting tracks through the magnet steel to the external drift chambers and by requiring a minimum energy deposition in the calorimeters.

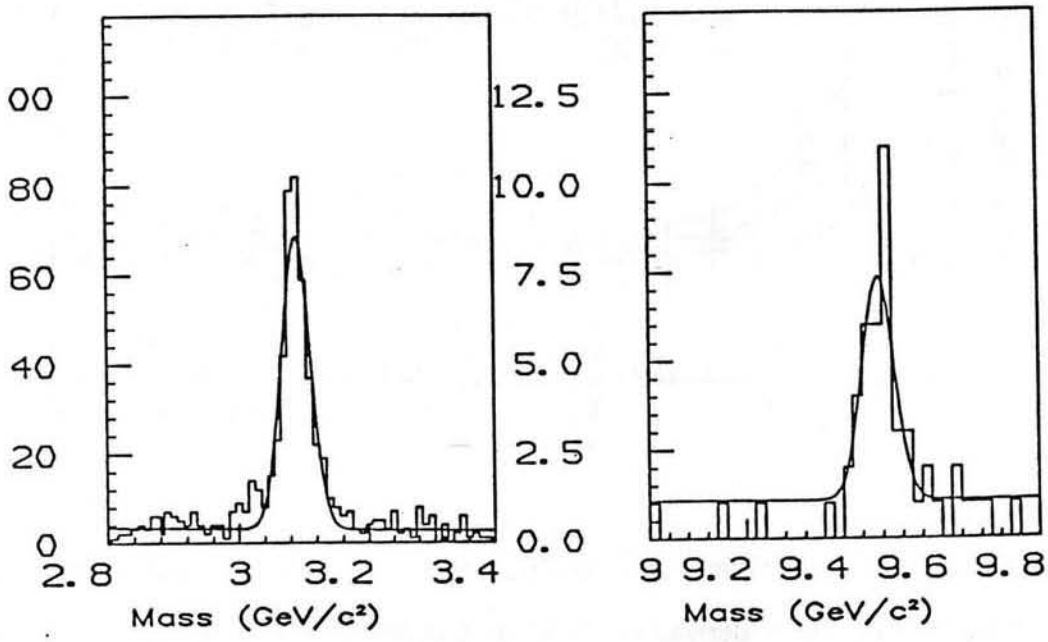

Figure 7 The CDF dimuon mass spectrum in the region of the ψ/J and the Υ. The fitted masses are 3.097 ± 0.001 and 9.469 ± 0.010 GeV respectively.

At CDF the calibration of the momentum measurement in the central tracking chamber is done with cosmic ray muons and is verified by studying the mass peaks for the ψ/J and Υ. The dimuon peaks for these two states are shown in Fig. 7. Fits to both peaks agree well with PDG averages. In fact as will be seen below, the best calibration of the tracking in the future will be obtained by comparing our Z mass value to the average value from LEP.

The electron energy measurement of the calorimetry is first calibrated using test beam electrons. This calibration is fine tuned in situ using electrons from W's and comparing their momentum from tracking with their calorimeter energy. Although the tracking has already been calibrated, there is a high probability that an electron will radiate some of its energy as it passes through the inner tracking chambers. The calorimeter will see the radiated photon and thus measures the total original energy of the electron. In Fig. 8 the ratio of E/p for W electrons is compared to a calculation which takes into account the radiative corrections to the momentum. This comparison is used to set the energy scale factor for the calorimetry. Because of the smaller statistics of the Z sample, this method results in a smaller scale uncertainty than a comparison of our Z signal to LEP.

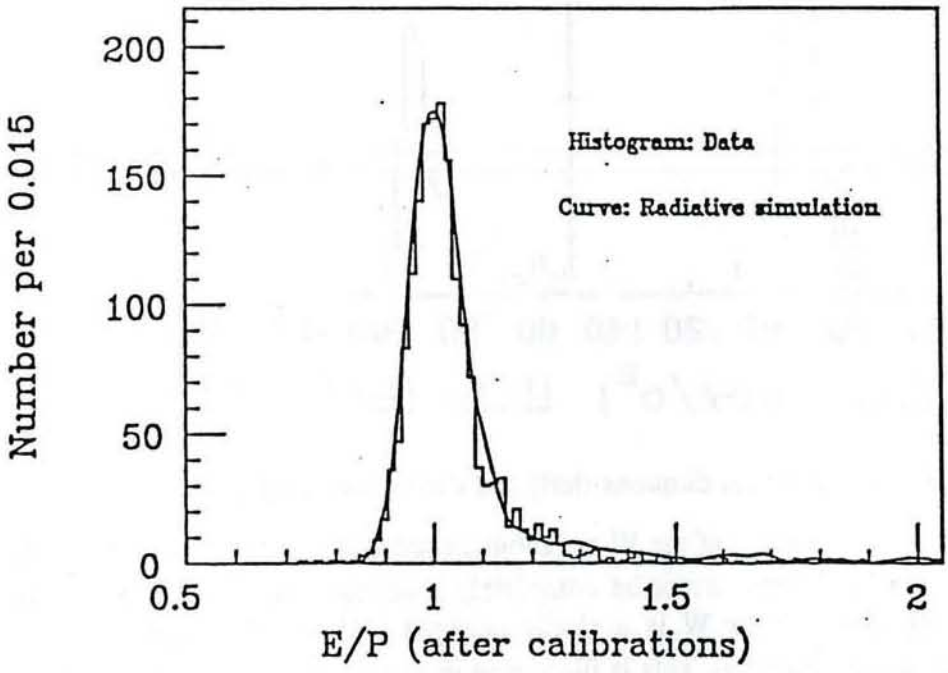

Figure 8 The ratio of calorimter energy to track momentum for electrons from W decays. The curve includes radiative corrections to the momentum.

The Z with its decay into two charged leptons is the easiest signal to measure. The CDF mass peaks for both the electron and muon channels [5] are shown in Fig. 9. The locations of the two peaks are in excellent agreement with each other, and the combined CDF result of $M_Z = 90.9 \pm 0.4$ GeV is in good agreement with the latest LEP average [6] of $M_Z = 91.18 \pm 0.03$ GeV. In future runs as our Z sample increases in size the latter comparison will become CDF's primary energy scale calibration.

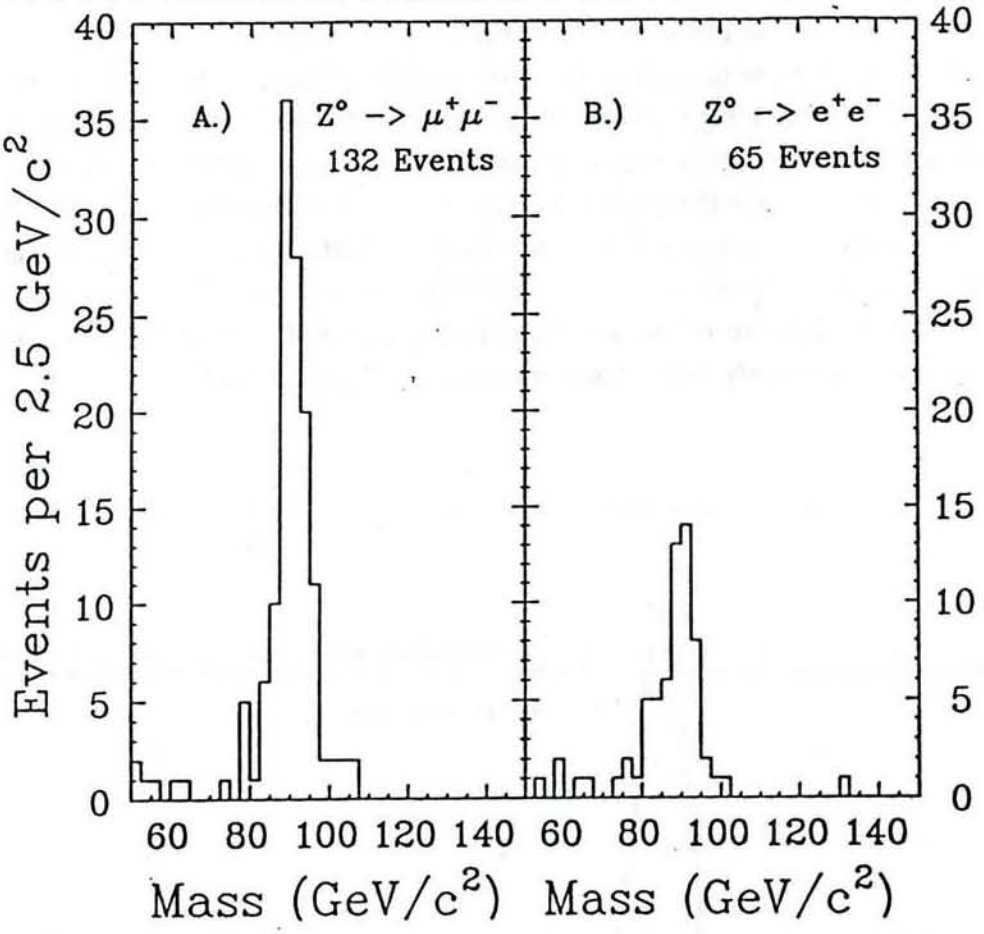

Figure 9 CDF Z mass peaks for dimuons (left) and dielectrons (right).

Although the leptonic decays of the W are about an order of magnitude more prolific than those of the Z, the W decays cannot be completely reconstructed because of the missing neutrino. The signature of the W is a single charged lepton with large E_T that is not balanced by any other visible E_T. This is illustrated in Fig. 10, where the E_T of the electron is plotted against the missing E_T for the W candidates in the electron channel. The events are roughly concentrated on a 45° line indicating that the electron E_T balances the missing E_T. Since the longitudinal momentum of the neutrino is not determined it is not possible to calculate the W mass directly. However, using only the transverse components of energy one can calculate a quantity called the transverse mass, $M_T = 2\, E_{Te}\, E_{T\nu}\, (1-\cos\Delta\phi)$, where $\Delta\phi$ is the azimuth angle separation of the electron and neutrino. This variable has a Jacobian peak at the W mass, and is relatively insensitive to the transverse momentum of the W itself. The M_T plots for the electron and muon W samples from CDF are shown in Fig. 11. The data samples shown here require a charged lepton with $E_T > 25$ GeV, missing energy with $E_T > 25$ GeV, no jet clusters with $E_T > 7$ GeV, and no extra tracks with $p_T > 15$ GeV. The latter two cuts are intended to improve the mass resolution of the sample.

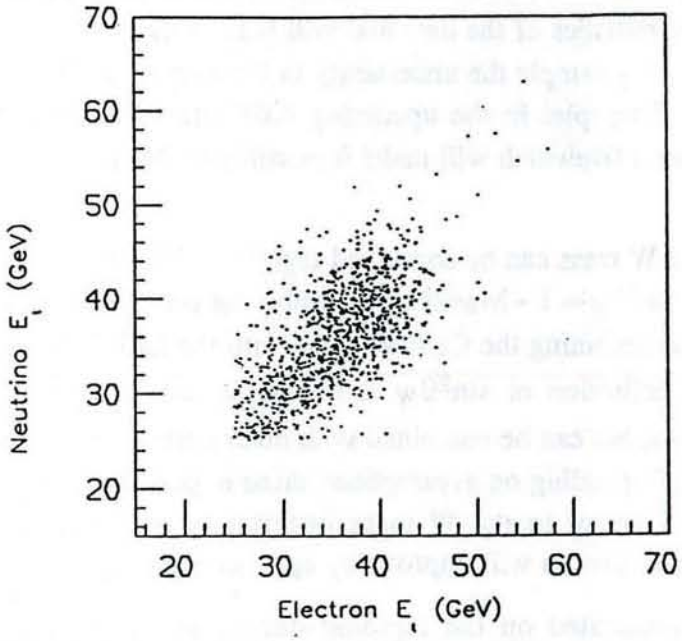

Figure 10 A scatter plot of missing E_T versus electron E_T for W candidates.

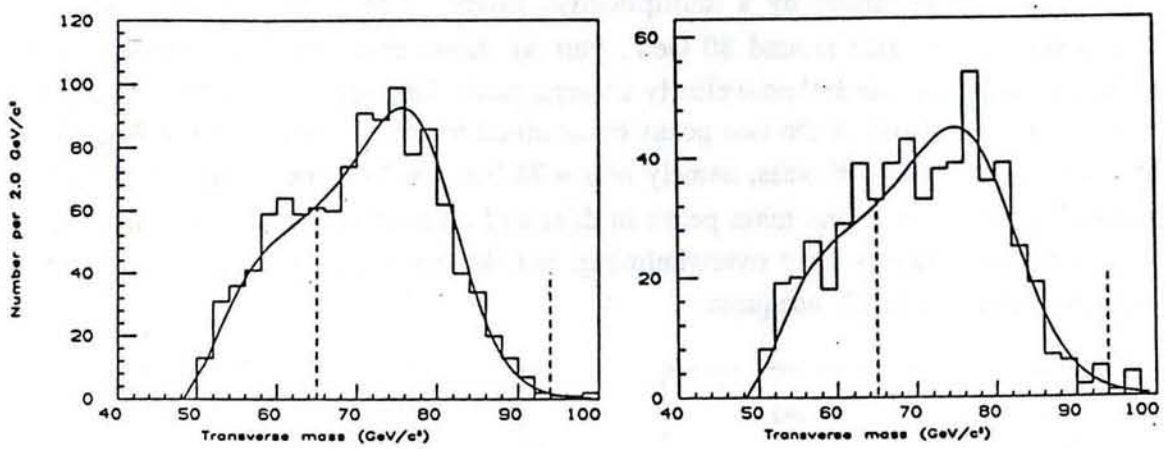

Figure 11 Transverse mass plots for the eν data (left) and μν data (right).

In order to determine the W mass from the data shown in Fig. 11 it is necessary to generate monte carlo simulations of the M_T spectrum for various values of M_W [7]. This monte carlo assumes the standard W production and decay dynamics and is done with a range of quark structure functions. The assumptions about experimental resolution come from both the test beam results and from other data samples. For example the "minimum bias" events taken with a total cross section trigger are used to determine the missing E_T resolution. Finally the W p_T distribution is calibrated against the Z sample. Although fits were attempted with the W width left as a second free parameter, the best results were obtained by fitting this to the nominal value of 2.1 GeV. The results of these fits for the electron and muon channels have comparable errors and are completely consistent with each other yielding a combined result of $M_W = 79.9 \pm 0.4$ GeV, when the error is a combination of statitistical and systematic uncertainties. This is to be compared with the UA2 result

[8] from electrons of $M_W = 80.5 \pm 0.5$ GeV. A large part of the quoted uncertainty in the CDF result depends on the statistics of the data and will benefit directly from the increased luminosity in future runs. For example the uncertainty in the energy scale will benefit from the increased size of the Z sample. In the upcoming CDF run the integrated luminosity should increase by a factor of five which will make it possible to decrease the uncertainty in M_W to about 0.2 GeV.

The measurement of the W mass can be combined together with the Z mass to obtain the weak mixing parameter, $\sin^2\theta_W = 1 - M_W^2/M_Z^2$. Combining the two CDF masses we get $\sin^2\theta_W = .231 \pm .008$, and combining the CDF W mass with the LEP Z mass we get .2317 $\pm$ .0075. This particular definition of $\sin^2\theta_W$ is not dependent on the top quark mass through radiative corrections, but can be combined with other derivations to obtain an upper limit on the top quark [9]. Depending on assumptions these upper limits range from 170 to 230 GeV. With the improvement in the W mass uncertainty in the next CDF run the accuracy of the $\sin^2\theta_W$ determination will improve by approximately a factor of two.

Although I have concentrated on the leptonic decays of the W and Z, the UA2 collaboration have taken advantage of their excellent calorimetry to observe the $\bar{q}$–q $\rightarrow$ dijet decay mode of these bosons [10]. Their data is shown is Fig. 12, where part a) shows the dijet mass spectrum enhanced by a multiplicative factor of M_{jj}^6. This factor makes it possible to see a small rise around 80 GeV. Part b) shows the same data divided by a smooth background estimate and now clearly shows a peak. This peak is then fitted to a pair of Gaussians with the ratio of the two peaks constrained to the nominal value of M_W/M_Z. The fit recovers the correct W mass, namely $M_W = 78.9 \pm 1.5$ GeV. This remarkable result shows how difficult it is to find mass peaks in dijet and multijet channels. Not only is the background from QCD processes overwhelming, but the mass resolution even under the best of circumstances is barely adequate.

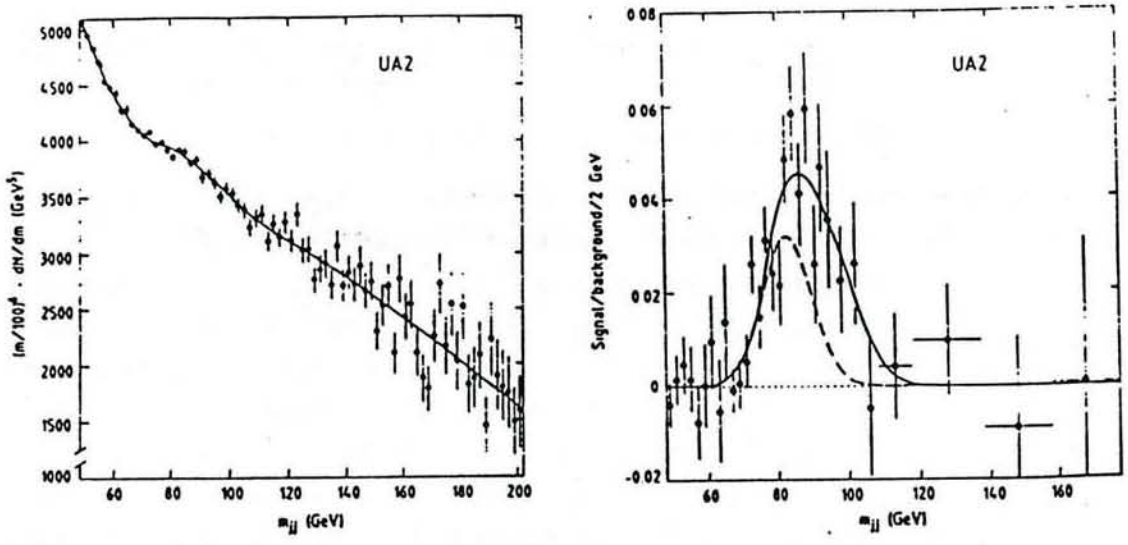

Figure 12 UA2 dijet mass data. Left hand figure has been enhanced by an M_{jj}^6 factor. Right hand figure has been divided by smooth background curve.

Turning to the production properties of the W and Z, in Fig. 13 the total cross sections are shown for UA2 and CDF energies [11]. The cross sections are in good agreement with a QCD prediction. The predominant uncertainty in the cross sections is in the integrated luminosity. An alternative way of presenting the results shown in Fig. 13 is to calculate the ratio, R, of the cross sections for the leptonic modes [12]. In this ratio the luminosity uncertainties cancel. Furthermore if one accepts the theoretical values for the boson total cross sections and leptonic widths then R depends only the ratio of the W and Z widths. Since LEP has measured the Z width very accurately, R becomes an indirect measurement of the W width. The CDF results for these quantities are $R = 10.2 \pm 0.9$ and $\Lambda_W = 2.19 \pm 0.20$ GeV.

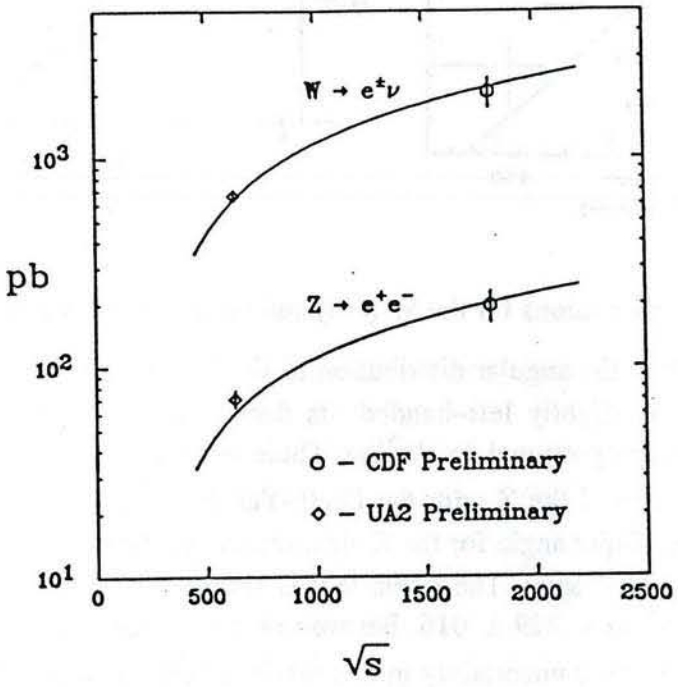

Figure 13 W and Z total leptonic cross sections from CDF and UA2.

The differential cross sections for W and Z production have also been measured and found to be in good agreement with QCD calculations. The CDF data is shown together with a QCD calculation by Reno and Arnold in Fig. 14. These data are obtained by relaxing the requirement that there be no additional jet activity in the events.

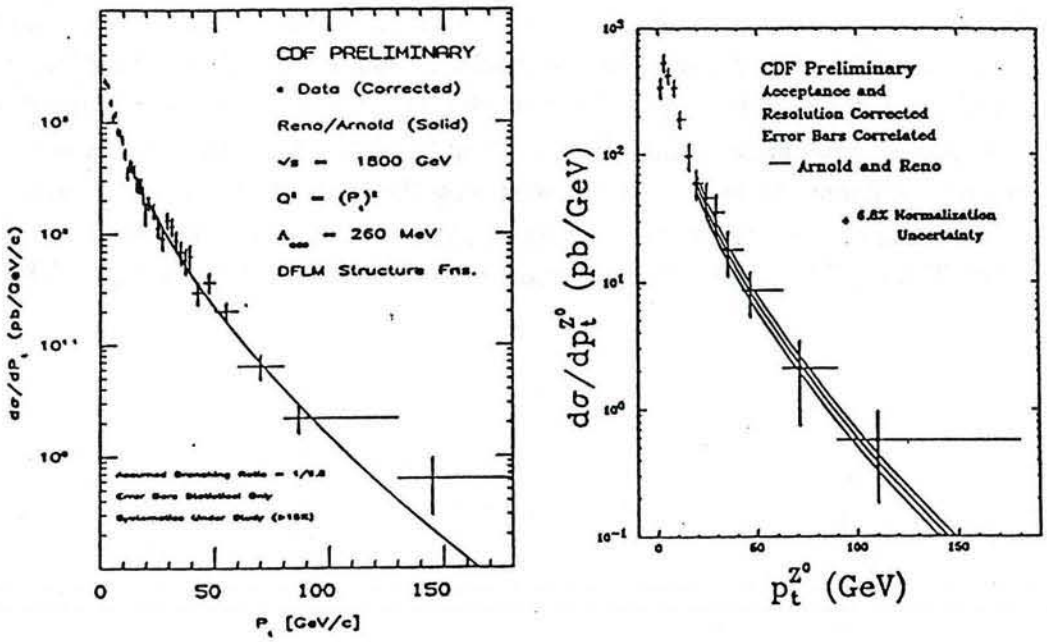

Figure 14 Differential cross sections for the W (left) and the Z (right) as a function of p_T.

Finally we take a look at the angular distribution of the Z decay, in particular the decay asymmetry. Since the Z is slightly left–handed, its decay distribution is expected to be asymmetric in an amount proportional to $\sin^2\theta_W$. There is also a small asymmetry which results from the interference of the Z with the Drell–Yan background. Fig. 15 shows the distribution of the Collins–Soper angle for the Z electron sample after corrections have been made for acceptance and efficiency. The curve that is shown is the result of a maximum likelihood fit yielding $\sin^2\theta_W = .229 \pm .016$. Because of the approximate charge symmetry of the experiment the systematic uncertainty in this result is very small and the quoted error is primarily statistical. This definition of $\sin^2\theta_W$ does depend on the top quark mass through radiative corrections. In Fig. 16 this result is transformed to the M_W/M_Z definition as a function of M_t. The M_W/M_Z results from CDF and UA2 are also shown. With the current level of statistics it is not yet possible to set a meaningful upper limit on the M_t, but this will improve in future runs. The W decay asymmetry, which is dependent on the structure functions and not on $\sin^2\theta_W$, is also currently being studied.

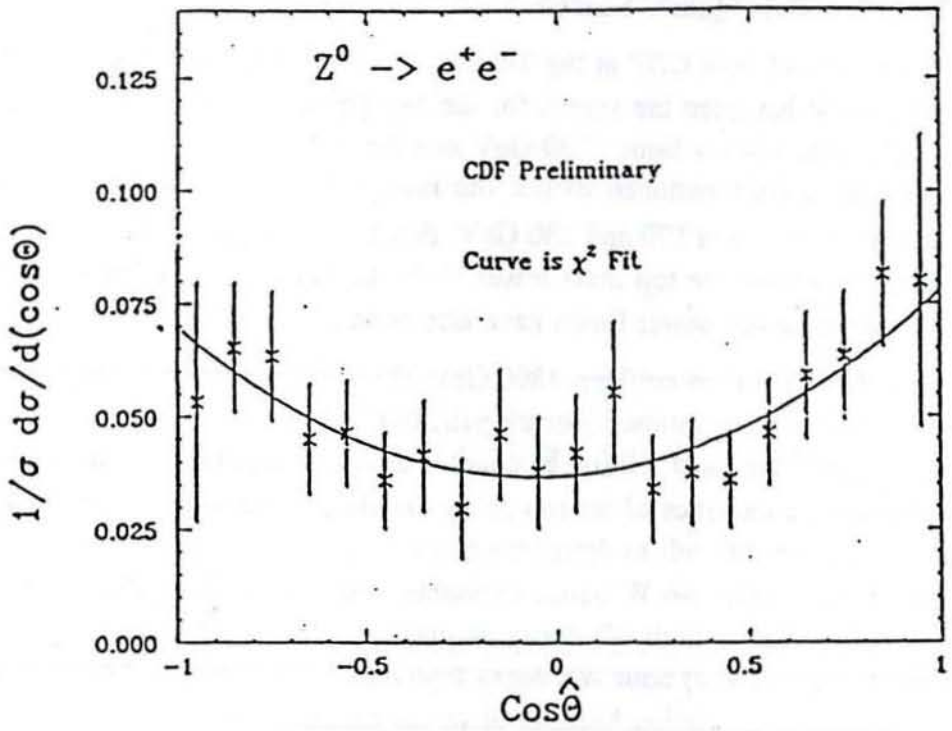

Figure 15 Z angular distribution as a function of the cosine of the center-of-mass angle (Collins–Soper representation).

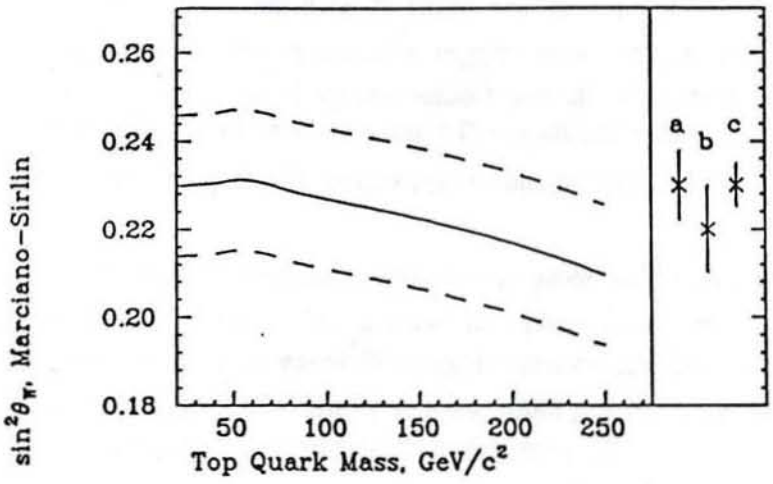

Figure 16 $\sin^2\theta_W$ as determined from the Z asymmetry versus top quark mass. The points on the right are $\sin^2\theta_W$ from M_W/M_Z: a) CDF, b) UA2, c) combined.

6. Heavy Flavors – Top Quark Search

In the previous runs of both CDF at the Tevatron collider and UA2 at the SPS collider the most exciting topic has been the search for the top quark. The absence of a toponium signal at Tristan had set a lower limit of 30 GeV and the earlier CERN collider results had raised this to 40 GeV. As mentioned earlier the interpretation of $\sin^2\theta_W$ also led to an upper limit somewhere between 170 and 230 GeV. From the data taken in the last CDF run it has been possible to raise the top mass lower limit above the W mass as I will discuss below. Similar, but somewhat lower limits have also been set by UA2.

At the energy of the Tevatron collider, 1800 GeV, the dominant mode for top production will be the production of a top antiquark–quark pair. Both top quarks will then decay to a W boson, which may be virtual, and a b (or $\bar{b}$) quark. For top quark masses comparable to or below the W mass, the kinematics of the top decay dictate that the W will carry away most of the energy. Hence it is difficult to detect the b quarks or their fragments and instead the top search must focus on the two W boson remnants. This means there are three possible topologies to be considered: a) both W's decay to quark jets, b) one W decays to jets and the other decays leptonically, and c) both W's decay leptonically. Possibility a) is very difficult as we noted in the previous section because of the large QCD background to the four jet system and because of the poor dijet mass resolution. For both b) and c) the identification of electrons and muons is the key issue just as in the last section .

As was previously discussed electrons are selected using both tracking and calorimetry information. Both must be completely consistent with an electron signal and consistent with each other. In addition cuts are made to eliminate γ and π° conversions, and E_T threshholds are imposed to ensure trigger efficiency. Finally an "isolation" cut is made which eliminates events where there are other energy depositions near the electron (any extra E_T in a surrounding cone with $R_{\eta\phi} = 0.4$ must be less than 5 GeV). This cut eliminates electrons from b quark production and decay, where the electron is accompanied by a nearby jet.

Likewise muons are selected by correlating a good track with either a track stub in the chambers outside the magnet steel or with a calorimeter cell with minimum energy deposition. A p_T threshhold ensures trigger efficiency as with the electrons, and a similar isolation cut is imposed. In the muon case not only does the isolation cut remove muons from b's, but it also reduces the probability of finding a secondary muon which results from the decay of one of the hadrons in a jet.

The first topology that I will discuss is the double semi–leptonic case, where both W's from the $\bar{t}$–t pair decay leptonically. Here the simplest signature is the production of two oppositely charged leptons. Although the branching ratio is small (2/81),the cleanest combination is to have one electron and one muon [13], which has neither any Drell–Yan background nor Z signals to cope with. The idea is to select events with an oppositely charged electron–muon pair with both leptons above the same E_T (or p_T) threshhold. Fig. 17 shows the predicted number of events above any threshhold between 5 and 40 GeV for

three different processes: direct $\bar{b}$–b production, $\bar{t}$–t production with M_t = 28 GeV, and $\bar{t}$–t with M_t = 70 GeV. The predictions were generated with ISAJET and assumed the integrated luminosity of the last CDF run. It can be seen that by setting the common threshhold at 15 GeV the $\bar{b}$–b background is completely eliminated, but reasonable efficiency for top masses up to 70 GeV is maintained.

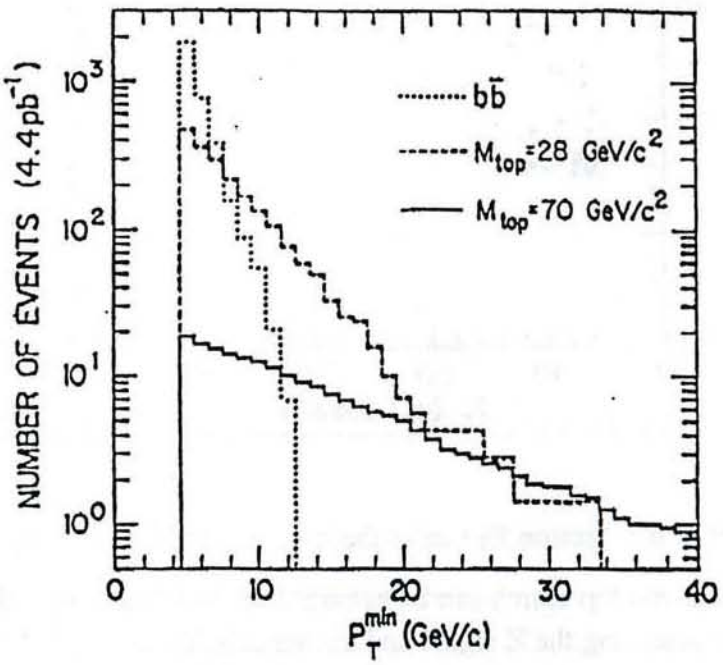

Figure 17 The number of events predicted by ISAJET to have both the electron E_T and the muon p_T greater than p_T^{min}. The curves are for $\bar{b}$–b and $\bar{t}$–t production as indicated.

A scatter plot of the electron E_T versus the muon p_T from the last CDF run is shown in Fig. 18. One event is observed above the dual 15 GeV threshholds. This event, although consistent with the interpretation as a $\bar{t}$–t decay, is located well above the threshholds, which is highly unusual with steeply falling spectra. Nonetheless if we assume that one event is observed then a 95% confidence level lower limit on the top mass is determined to be 72 GeV. This limit takes the efficiencies for detecting and reconstructing the two leptons fully into account.

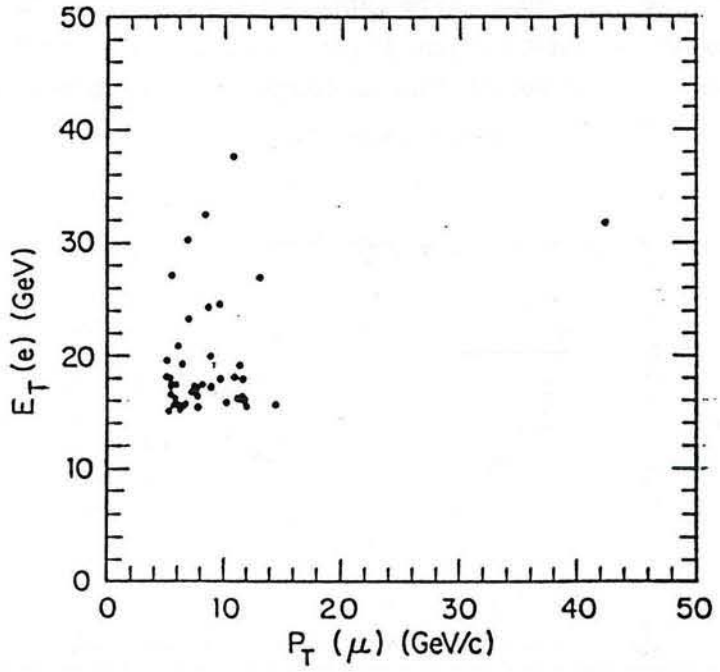

Figure 18 Scatter plot of the electron E_T versus the muon p_T for the CDF data.

The double semi–leptonic top search can be extended by including the dielectron and and dimuon channels after removing the Z signal and accounting for the Drell–Yan background. The Z is removed by a mass window cut from 75 to 105 GeV; in addition it is required that the missing E_T be greater than 20 GeV and the charged leptons not be back to back in azimuth. After these cuts are made, the addition of these channels increases the acceptance for the top signal by about 50%. No new events are observed to pass the cuts, and as a result the lower limit is raised to 84 GeV (95% C.L.). It is also possible to increase the top acceptance an additional 15% by extending the electron angular acceptance to include the plug gas tube calorimeter. With this extension the lower limit becomes 87 GeV (95% C.L.). Both of these extensions to the published CDF limit are still preliminary, but it is important to note that they require the top quark mass to be significantly above the W mass. Hence the W in the top quark decay will be on the mass shell, which has direct consequences for the search methodology in the future.

We now turn to the single semi–leptonic channel where the second t (or $\bar{t}$) quark decays into two quark jets. The branching ratio for this channel is higher than for the double semi-leptonic, but there is now a major background, namely QCD production of the W plus two jets. The initial studies of this channel used the transverse mass variable to look for enhancements below the W jacobian peak [14]. The data sample required that there be an electron and missing energy both with $E_T > 20$ GeV, plus two (or more) jets both with $E_T >$ 10 GeV. The published 95% C.L. lower limits obtained by this method were 69 GeV for UA2 and 77 GeV for CDF.

Now that it appears certain that the top mass is above M_W, the transverse mass is no longer a useful tool to investigate the single semi-leptonic events. Another possibility is to look for a W mass peak in the accompanying dijets, but as we have noted in section 5 this is extremely difficult and does not provide a unique $\bar{t}$–t signature. Therefore it is necessary to find evidence of the b or $\bar{b}$ quark fragments. A first attempt at this has been done by searching for a soft muon resulting from the b decay. In addition the single semi-leptonic sample has been expanded to include primary muons as well as electrons. The extra soft muon is required to have $p_T > 1.7$ GeV, and must be separtated from the nearest W jet by $R_{\eta\phi} > 0.5$ to eliminate punch–through. No events are observed with these extensions to the analysis. When this result is combined with the double semi–leptonic results the 95% C.L. lower limit on the top mass is raised to 91 GeV. This preliminary result is shown in Fig. 19, where the upper limit on the $\bar{t}$–t cross section as measured by CDF is plotted for each of the successive analysis steps described above. The intersection of each of these curves with the lower limit of the of the QCD prediction for $\bar{t}$–t production gives the corresponding top mass limit.

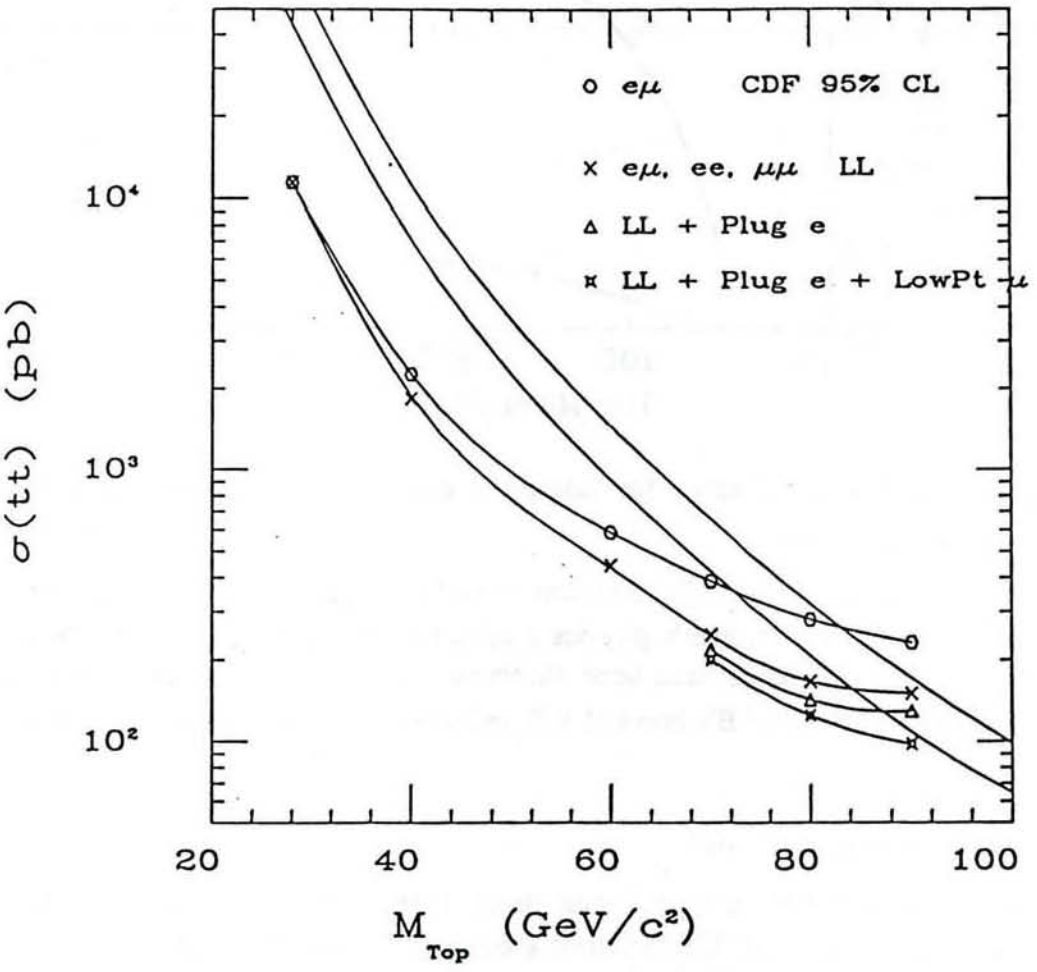

Figure 19 The preliminary CDF upper limits on the $\bar{t}$–t cross section as a function of the top quark mass for the sequential analyses described in the text. The pair of smooth curves give the limits of the theoretical prediction.

In the next CDF run if we are unlucky enough to find no additional events with the same analyses as described above, then the measured cross section upper limits shown in Fig. 19 will be lowered in inverse proportion to the increase in integrated luminosity. For example if we receive a fivefold increase in luminosity, the extrapolation of these curves would indicate a M_t lower limit around 120 GeV. However, we also plan to improve the analyses, in particular by taking advantage of the increased energy of the b and $\bar{b}$ fragments with larger M_t. With the addition of a silicon vertex detector it should be possible to directly tag many of the b decays. An estimate of the efficiency of the b tagging as a function of M_t is shown in Fig. 20. Furthermore the extended muon coverage in the next run will improve the acceptance for both primary and secondary muons. With these improvements we expect to push the top mass limit well above 120 GeV.

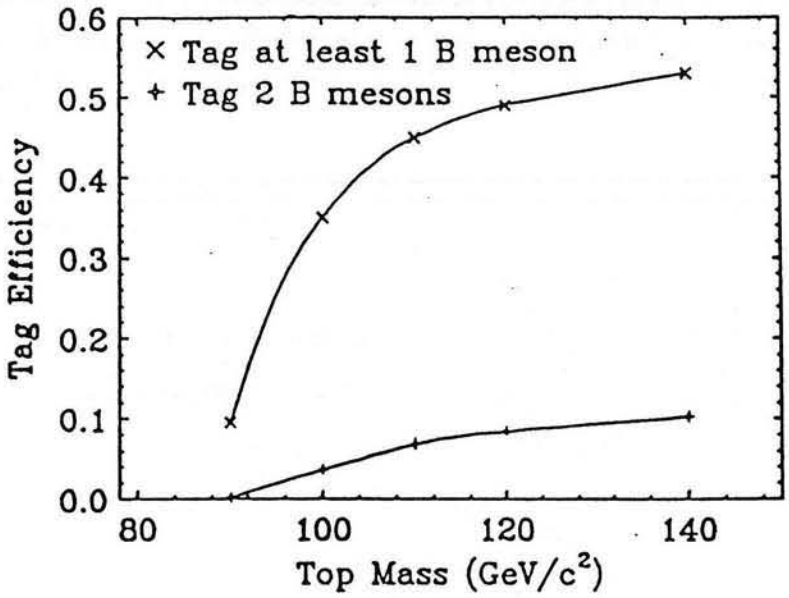

Figure 20 The predicted efficiency for tagging B mesons with the new silicon vertex detector in the next CDF run.

Having mentioned b tagging it is important to add that CDF will also utilize the new silicon vertex detector for extensive b–physics studies in the next run. In the data from the previous run Υ, Υ', and Υ'' peaks have been observed in the dimuon channel. We are also studying the inclusive decays of B's into $\psi/J + X$ and other states as well as $\bar{B}B$ mixing.

7. Beyond the Standard Model

Although several searches for unorthodox states have taken place I will just mention two. First we have searched the dilepton mass spectra above the W and Z for higher mass gauge bosons. Aside from a couple of very high mass events, there is no evidence for any peak. Assuming standard couplings for such states, lower mass limits are found to be $M_{W'} > 380$ GeV and $M_{Z'} > 400$ GeV (95% C.L.).

Second, multijet events with large missing E_T are a possible signature of supersymmetric squarks and gluinos decaying to stable, undetected photinos plus hadrons. CDF has an sample of 98 events with missing $E_T > 40$ GeV which, however, can be fully explained by W and Z production and QCD multijets [15]. The resulting squark and gluino mass limits are shown in Fig. 21. The limits are worse for the case where the gluino is lighter than the squark because the final decay to a photino state is three–body and not two–body.

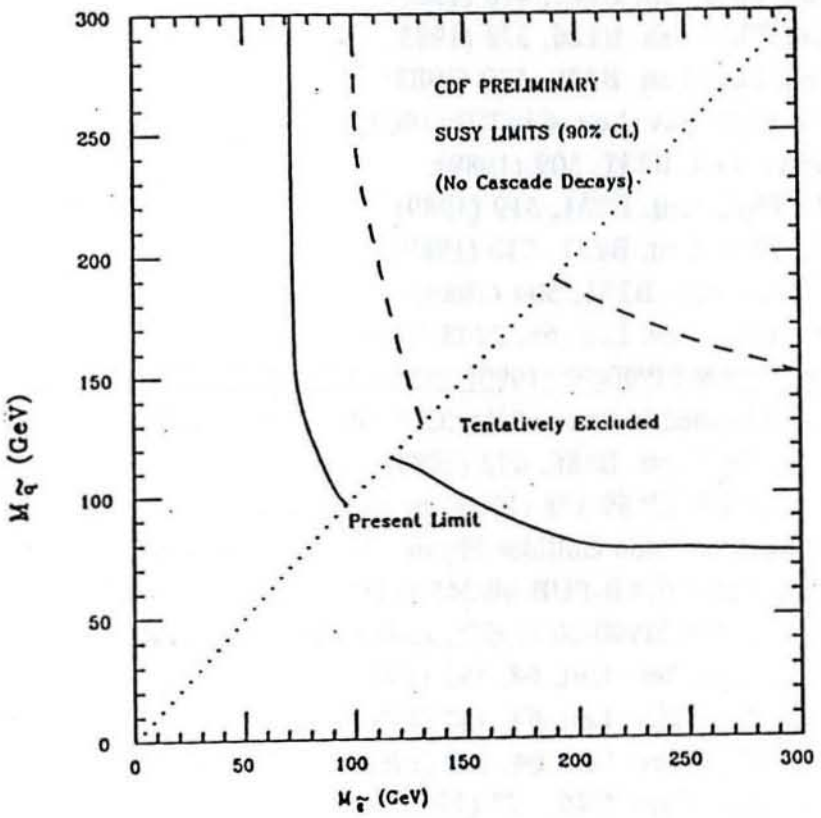

Figure 21 The mass limits for squarks (vert.) versus gluinos (horiz.) as obtained by CDF.

I would like to thank the organizers of the 5th Nishinomiya Yukawa–Memorial Symposium for their kind invitation and hospitality. I would also like to thank my CDF colleagues for their help with the preparation of this talk.

References

1. CDF Collaboration, NIM **A271**, 387 (1988).
2. S.D. Ellis, A. Kunst and D. Soper, Phys. Rev. Lett. **62**, 726 (1989).
3. CDF Collaboration, Phys. Rev. Lett. **62**, 3020 (1989).
4. UA1 Collaboration, Phys Lett. **B122**, 103 (1983);
   UA2 Collaboration, Phys Lett. **B122**, 476 (1983);
   UA1 Collaboration, Phys Lett. **B126**, 398 (1983);
   UA2 Collaboration, Phys Lett. **B129**, 130 (1983).
5. CDF Collaboration, Phys. Rev. Lett. **63**, 720 (1989).
6. B. Adeva *et al.*, Phys. Lett. **B231**, 509 (1989);
   D. Decamp *et al.*, Phys. Lett. **B231**, 519 (1989);
   M. Akrawy *et al.*, Phys. Lett. **B231**, 530 (1989);
   P. Aarnio *et al.*, Phys. Lett. **B231**, 509 (1989).
7. CDF Collaboration, Phys. Rev. Lett. **65**, 2243 (1990).
8. UA2 Collaboration, CERN EP/90-22 (1990), submitted to Phys. Lett. **B**.
9. P. Langacker, to be published in Proc. of PASCOS-90, Boston, 1990.
10. UA2 Collaboration, Phys Lett. **B186**, 452 (1987);
    UA2 Collaboration, CERN EP 89-178 (1989), to be published in Proc. of 8th Topical Workshop on Proton Antiproton Collider Physics, Castiglione, 1989.
11. CDF Collaboration, FERMILAB-PUB-89/245 (1989), submitted to Phys. Rev. Lett.;
    UA2 Collaboration, CERN EP/90-20 (1990), submitted to Phys. Lett. **B**.
12. CDF Collaboration, Phys. Rev. Lett. **64**, 152 (1990).
13. CDF Collaboration, Phys. Rev. Lett. **64**, 147 (1990).
14. CDF Collaboration, Phys. Rev. Lett. **64**, 142 (1990);
    UA2 Collaboration, Zeit. Phys. **C46**, 179 (1990).
15. CDF Collaboration, Phys. Rev. Lett. **62**, 1825 (1989).